

The resistance of Cu nanowire–nanowire junctions and electro-optical modeling of Cu nanowire networks

Cite as: Appl. Phys. Lett. **116**, 251902 (2020); doi: 10.1063/5.0012005

Submitted: 27 April 2020 · Accepted: 10 June 2020 ·

Published Online: 23 June 2020



View Online



Export Citation



CrossMark

Hugh G. Manning,^{1,2,a)} Patrick F. Flowers,³ Mutya A. Cruz,³ Claudia Gomes da Rocha,⁴ Colin O' Callaghan,⁵ Mauro S. Ferreira,^{2,5} Benjamin J. Wiley,³ and John J. Boland^{1,2}

AFFILIATIONS

¹School of Chemistry, Trinity College Dublin, Dublin 2, Ireland

²Advanced Materials and Bioengineering Research (AMBER) Centre, Trinity College Dublin, Dublin 2, Ireland

³Department of Chemistry, Duke University, Durham, North Carolina 27708-0354, USA

⁴Department of Physics and Astronomy, University of Calgary, 2500 University Drive NW, Calgary, Alberta T2N 1N4, Canada

⁵School of Physics, Trinity College Dublin, Dublin 2, Ireland

^{a)}Author to whom correspondence should be addressed: manninh@tcd.ie

ABSTRACT

Flexible transparent conductors made from networks of metallic nanowires are a potential replacement for conventional, non-flexible, and transparent conducting materials such as indium tin oxide. Cu nanowires are particularly interesting as cost-effective alternatives to Ag nanowires—the most investigated metallic nanowire to date. To optimize the conductivity of Cu nanowire networks, the resistance contributions from the material and nanowire junctions must be independently known. In this paper, we report the resistivity values (ρ) of individual solution-grown Cu nanowires (ρ) = 20.1 ± 1.3 n Ω m and the junction resistance (R_{jxn}) between two overlapping Cu nanowires (R_{jxn}) = 205.7 ± 57.7 Ω . These electrical data are incorporated into an electro-optical model that generates analogs for Cu nanowire networks, which accurately predict without the use of fitting factors the optical transmittance and sheet resistance of the transparent electrode. The model's predictions are validated using experimental data from the literature of Cu nanowire networks composed of a wide range of aspect ratios (nanowire length/diameter). The separation of the material resistance and the junction resistance allows the effectiveness of post-deposition processing methods to be evaluated, aiding research and industry groups in adopting a materials-by-design approach.

© 2020 Author(s). All article content, except where otherwise noted, is licensed under a Creative Commons Attribution (CC BY) license (<http://creativecommons.org/licenses/by/4.0/>). <https://doi.org/10.1063/5.0012005>

Metallic nanowire networks (NWNs) provide a route to highly transparent, highly conductive, flexible, easy-to-fabricate, and low-cost materials.¹ The large-scale integration of these materials into commercial devices could revolutionize display, touch screen, as well as numerous emerging applications.² To assess the true potential of metallic NWN systems, it is crucial to establish a complete understanding of their individual physical properties and how these properties affect the performance of the network.³ This requires a part-to-whole consideration of the network, evaluating and characterizing each aspect of the system, such as the ability of the nanowire (NW) to conduct electrical charge and the electrical resistance at each of the NW junctions within the network. While Ag NWNs have their merits, the high-cost, susceptibility to corrosion, and the potential

future scarcity of Ag could prohibit their widespread adoption.⁴ On the other hand, Cu in bulk form is only 6% less conductive than Ag, but 1500 times more abundant and 87 times cheaper.⁵ Over the past number of years, there has been a large amount of interest in using Cu NWs in composite materials and conducting networks.⁶ Cu NWs are also promising candidates as interconnects in future nanodevices.⁷ While the study of Cu NWNs is much less developed than their Ag counterparts, recent developments in Cu NW synthesis have allowed NWs with aspect ratios (ARs) (length/diameter) as high as 5700 to be grown, which has allowed the fabrication of flexible transparent conductors with sheet resistance (R_s) performances of 50 Ω/\square at 90% optical transmittance (T), making them viable alternatives to Ag NWNs.⁸

The performance of any network is not just dependent on the materials used but how the network is processed; this influences the properties of the nanowires and the junctions that comprise the network. The resistance of Ag NW junctions has been previously established^{9,10} and has enabled the comparison of post-processing conditions, which remove the insulating polymer coating from the polyol synthesis method and assist in the development of accurate computational models predicting the performance of Ag NWN-based materials.^{11,12} One drawback of Cu NWs is that they readily oxidize in ambient conditions, insulating the conducting core and causing a large contact resistance at each of the nanowire–nanowire junctions. Post-processing methods have been developed to remove the oxide layer, which include acetic acid washes, plasma cleaning, high-temperature hydrogen annealing, and photonic welding.^{13,14}

In this paper, we present the electrical measurements of solution-grown Cu NWs, allowing the determination of the material resistivity (ρ) and junction resistance (R_{jxn}). Electrical characterization of these fundamental material properties enables the use of a multi-nodal representation (MNR) electro-optical computational model to predict R_s and T as a function of R_{jxn} . Exploiting the electrical properties of individual Cu NWs and their junctions enables efficient comparison, optimization, benchmarking, and modeling of the corresponding NWN material.

Pentagonally twinned Cu NWs were synthesized using the method described by Rathmell and Wiley.¹⁵ To remove polyvinylpyrrolidone (PVP) and diethylhydroxylamine (DEHA), the NWs were transferred into a volatile solvent using the following protocol. Disperse the NWs by shaking. Take a sample of the NWs, centrifuge at 2000 RPM for 3 min, and remove the supernatant. Using a 1 wt. % DEHA solution, the NWs were rinsed three times to remove PVP. The NWs were rinsed with ethanol (EtOH) to remove water and DEHA. NWs were then rinsed with isopropyl alcohol (IPA) to remove EtOH. Finally, the NWs were suspended in IPA at the desired concentration. Figure S1 presents transmission electron microscopy (TEM) analysis of the Cu NWs, showing what appear to be stacking faults and a native oxide coating with noticeable surface roughness. Figure S1 also shows distributions of the length ($20.2 \pm 12.5 \mu\text{m}$) and diameter ($84 \pm 18 \text{ nm}$) and the diameter-dependent native oxide, which forms on the surface of the wire. No significant length–diameter correlation was observed (Fig. S2).

Experiments were carried out on p-type silicon wafers (University Wafer) with a 300 nm thermally grown SiO_2 layer; the Cu NW solution was drop-cast onto substrates pre-patterned by UV lithography. Single and crossed Cu NWs were fabricated by electron-beam lithography (EBL) using previously reported techniques with 120 nm of electron beam-evaporated Ag as the electrode material.⁹ Scanning electron microscopy (SEM) imaging and EBL were performed using a Zeiss Supra FEG-SEM. TEM images were acquired using a FEI TITAN TEM. Electrical measurements were taken in ambient conditions on a Keithley 4200 SCS.

MNR simulations were carried out by solving Kirchhoff's circuit equations numerically. The model and the code are described in detail and are available in an earlier publication.¹¹ For predicting the performance of Cu NWNs, the material resistivity was set at $\rho = 20.1 \text{ n}\Omega \text{ m}$, while R_{jxn} was varied according to experiment. The extinction cross section, C_{ext} , was calculated using the MatScat (Mie theory for infinite cylinders) implementation by Schäfer *et al.*¹⁶ using various values of

the NW diameter and the optical constants for Cu, $n = 1.0344$ and $k = 2.57984$ at $\lambda = 546 \text{ nm}$.¹⁷ C_{ext} is converted into Q_{ext} , the extinction efficiency, by dividing by the NW diameter (the 1D optical cross section). A plot of Q_{ext} vs diameter for Ag and Cu can be found in the [supplementary material](#) (Fig. S3).

Due to the insulating nature of the Cu NW native oxide shell and the electrochemically active Cu core, when a pair of Ag electrodes are put into contact with a single NW and a sufficiently high voltage is applied, resistive switching can occur at the wire-electrode interface. Cu and Ag are widely used as an oxidizable (soluble) electrode in many metal–electrolyte–metal (MEM) or metal–insulator–metal (MIM) thin-film devices.¹⁸ Electroforming involves applying a positive voltage to the oxidizable electrode, which leads to the dissolution of the metal, migration through the insulating layer, and deposition of a metallic filament at the opposite electrode. As more material is deposited, a “virtual cathode” grows back through the oxide toward the anode and ultimately bridges the two electrodes.¹⁹ The voltage this occurs at is defined as V_{SET} , defining a low-resistance ON state (LRS). The resistance of the LRS can be set by limiting the current compliance. When the current compliance is removed and sufficient current (I_{RESET}) is driven through the nanoscale filament in the LRS, Joule heating causes a thermal dissolution of the filament and the conducting bridge is disconnected, establishing a high-resistance OFF state (HRS) by unipolar resistive switching.²⁰ The junction activation process in a network of oxide-coated Cu NWs has been shown to result in a winner-takes-all conducting path formation.²¹ Furthermore, CuO_x NWs have demonstrated forming-free non-volatile resistive switching and memristive effects.²² A further study is warranted on these types of materials as they could enable flexible transparent memories and multi-functional devices.

Establishing a stable low-resistance Ohmic contact between the EBL-defined electrodes [Fig. 1(a)] and the Cu core requires electroforming the connections. Figure 1(b) displays an I – V plot where voltage sweeps are performed at an increasing current compliance value and the LRS is not retained after the SET event. This is known as threshold switching and commonly occurs at low current compliance limits,²³ and a plot of the threshold and LRS SET voltage vs current compliance for seven single nanowire devices and three nanowire junctions can be found in the [supplementary material](#) (Fig. S4). In this device, with a current compliance of $120 \mu\text{A}$, the sample demonstrated a stable low-resistance (419Ω) Ohmic response. NWs, which were typically put in a LRS using a current compliance of a few $100 \mu\text{A}$ s, could be resistively switched to the HRS through unipolar behavior at a current value of $\sim 1 \text{ mA}$. After each pair of electrodes had been electroformed to a LRS, the resistance of the NW was measured using the four-probe method. High-resolution SEM allowed the measurement of the NW diameter, with the length of the device taken from the outer-most edge of the inner two electrodes [Fig. 1(a)] when calculating the material resistivity, ρ , as per Kolečník *et al.*²⁴

The thickness of the native oxide was accounted for in the diameter of the NW using the linear dependence of the oxide thickness on the diameter (D) observed by TEM [Fig. S1(e)]. The ρ values for six samples were calculated and are plotted in Fig. 1(c). The mean resistivity $\langle \rho \rangle = 20.1 \pm 1.3 \text{ n}\Omega \text{ m}$ (blue dashed line) is closer to the bulk value than previously measured solution grown-Cu NWs ($35 \text{ n}\Omega \text{ m}$),⁷ but higher than electrodeposited and highly twinned Cu NWs ($17.8 \text{ n}\Omega \text{ m}$).²⁵ The bulk ρ value for Cu is shown as the red dashed line in

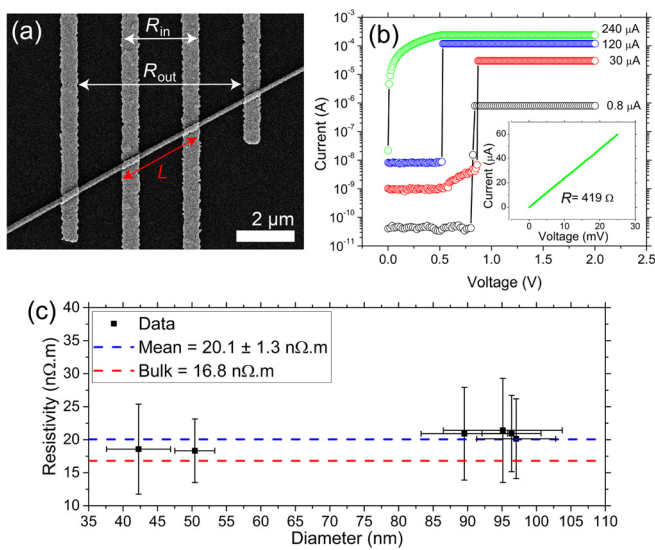


FIG. 1. Electroforming for Ohmic conduction in a single Cu NW. (a) SEM image of a single Cu NW in contact with four electrodes for resistivity (ρ) measurements. The inner and outer electrodes are identified for the four-probe measurement. (b) I-V curve showing the electroforming process by increasing current compliance. The inset curve shows the low resistance ($419\ \Omega$) Ohmic response after electroforming. (c) ρ values for six individual NWs of varying diameters, with error bars originating from the standard deviation of ten measurements of the NW diameter. The ρ value for bulk Cu is shown by the red dashed line at $16.8\ \text{n}\Omega\cdot\text{m}$. Cu NW $\langle\rho\rangle$ is plotted by the blue dashed line at $20.1 \pm 1.3\ \text{n}\Omega\cdot\text{m}$.

Fig. 1(c) with a value of $16.8\ \text{n}\Omega\cdot\text{m}$. Compared to measurements for Ag NWs ($20.3 \pm 5.5\ \text{n}\Omega\cdot\text{m}$),⁹ our results show a no appreciable difference in the conductivity of solution-grown Cu NWs and Ag NWs.

Establishing the Cu NW ρ is crucial to accurately calculating the junction resistance R_{jxn} . As in the case of the single NW measurements, an electroforming procedure was run between each of the contacts (electrodes 1–2 and 3–4) to the NW on either side of the junction and then to the junction itself (electrodes 2–3) [Fig. 2(a)]. Bringing the junction into a LRS involves creating a conductive filament through both oxide shells [Fig. 2(b)].

The electroforming process is carried out in the same manner as that used in the activation of the electrical contacts on a single Cu NW. The voltage is linearly increased until a SET event occurs, and the current flow across the device quickly increases until it reaches the limiting current compliance (1 mA in this case). Through this process, the device is taken from the pristine HRS to a LRS [Fig. 2(c)]. The inset schematic illustrates the conductive filament, which bridges the two metallic NW cores. The inset I-V curve shows the two-point Ohmic response of the NW junction after electroforming with a resistance value of $1150\ \Omega$. After a stable electrical connection is established for all the EBL-defined contacts and the junction, a four-probe measurement of the crossed NW structure can be performed.

Removing the resistance contributions from the NW lengths up to the junction involves the same calculation as previously described for Ag NW junctions,⁹ but with one difference, the oxide thickness is removed from the measured D of the NW as it does not contribute to electrical conduction. The graph shown in Fig. 2(d) shows the R_{jxn} measurements for three individual Cu NW junctions. $\langle R_{\text{jxn}} \rangle$ was

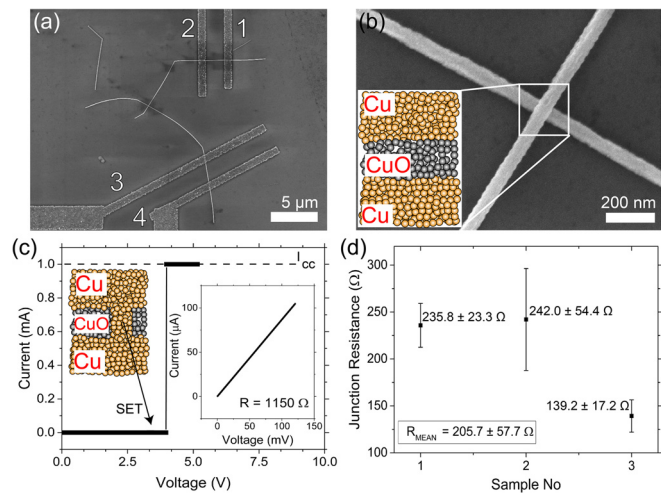


FIG. 2. Cu NW R_{jxn} measurement. (a) SEM image of a Cu NW junction contacted for the four-probe measurement. (b) Magnified SEM of the NW junction. The inset schematic illustrates the metal-insulator-metal structure of the junction in the pristine, non-conductive state. (c) Electroforming I-V curve for the NW junction, with a current compliance of 1 mA. The inset graph shows the resistance of a subsequent two-probe measurement with a resistance of $1150\ \Omega$. The top-left inset schematic depicts the Cu conductive bridge formed through the oxide. (d) Measurements on three individual junctions yield $\langle R_{\text{jxn}} \rangle = 205.7 \pm 57.7\ \Omega$.

calculated to be $205.7 \pm 57.7\ \Omega$, significantly higher than the median value for Ag NW junctions, $\langle R_{\text{jxn,Ag}} \rangle = 11\ \Omega$.⁹

We recently published a method that accurately describes the electrical and optical performance of Ag NWNs using a multi-nodal representation (MNR) of a NWN, that is, considering both the resistance contribution of the NW junctions and the NW segments between them, coupled with an optical model based on Mie light scattering theory (MLST).¹¹ The electrical results presented above allow the MNR and MLST model to be applied to Cu NWs, predicting the electro-optical performance of a Cu NWN transparent conductor electrode using only physical properties such as the NW length (L) and diameter (D), electrical parameters such as $\langle\rho\rangle$ and $\langle R_{\text{jxn}} \rangle$, and the optical constants of Cu. By choosing physical parameters that match datasets already published in the literature, we can test the MNR and MLST model on its predictive accuracy. If the *ab initio* model predicts data consistent with experimental observation, it would be a powerful tool to forecast, benchmark, and design Cu NWNs for specific purposes. Furthermore, the average R_{jxn} component of R_s can be varied to determine the efficacies of post-processing techniques, synthesis methods, and deposition procedures and to assess the ultimate performance of the NWN as $R_{\text{jxn}} \rightarrow 0$.

Figure 3 displays the experimental and computationally predicted datasets of four Cu NWN systems with aspect ratios (ARs) ranging from 330 to 1860. For each set of simulations, L and D values were set to match the NW dimensions reported by the authors in the experimental measurements. Simulations were performed with three values of $\langle R_{\text{jxn}} \rangle$, $205\ \Omega$, representing the average R_{jxn} measured in this work, $100\ \Omega$, and a “highly optimized” $\langle R_{\text{jxn}} \rangle$ value of $1\ \Omega$. These $\langle R_{\text{jxn}} \rangle$ values are plotted in red, blue, and green, respectively. Figures 3(a) and 3(b) present the experimental results of Borchert *et al.* where Cu NWs with ARs of 330 and 570 were dispersed in a nitrocellulose-based ink

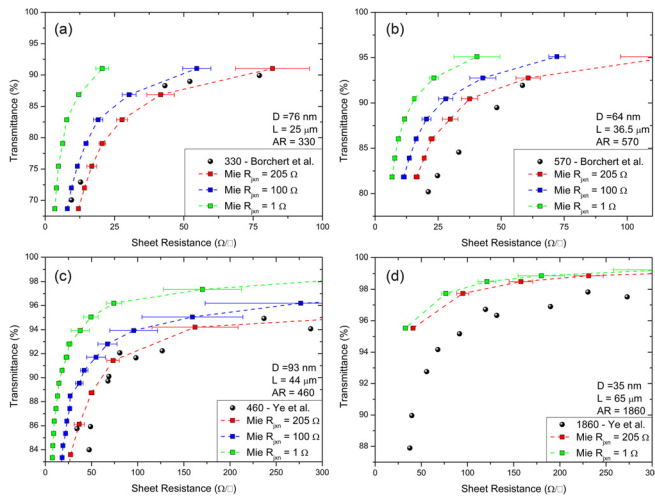


FIG. 3. Transmittance vs sheet resistance, experimental and simulated predictions for four datasets of Cu NWNs. (a)–(d) The black circular points on each panel represent experimental data of Cu NWNs from reported literature values, with the diameter (D), length (L), and aspect ratio ($AR = L/D$) for each dataset detailed on the right of each graph.^{8,13} The colored square datapoints show the predictions of the MNR and MLST model where, in red, $R_{jxn} = 205 \Omega$, in blue, $R_{jxn} = 100 \Omega$, and in green, $R_{jxn} = 1 \Omega$. The error bars at each of the simulation datapoints show the standard deviation of R_s for ten simulated network samples.

and printed onto polyethylene terephthalate (PET) using a Meyer rod, respectively. The films were subjected to a $4\times$ repeated rinsing with acetic acid to improve R_s . The authors used a Monte Carlo model, which approximates that R_s originates from R_{jxn} only and includes L dispersivity to fit experimental data. Through this method, they extracted a lower boundary for $R_{jxn} \sim 2 \text{ k}\Omega$ and an upper boundary for $R_{jxn} \sim 10 \text{ k}\Omega$ with no modeling of the optical properties.¹³ The MNR and MLST model predicts the R_s and T of the networks with close agreement with the experimental data in the case of $AR = 330$, slightly overpredicting the performance for $AR = 570$. Figures 3(c) and 3(d) display the experimental data from the study by Ye *et al.* who fabricated Cu NWs of $AR = 460$ and 1860 , respectively. For larger aspect ratio systems, T exhibits a less dependence on R_{jxn} . This is due to a decrease in junction density with increasing L ¹² and a reduction of Q_{ext} with decreasing D . All Cu NWN films were deposited by Meyer rod coating and plasma cleaned and annealed in a tube furnace for 30 min at 225°C .⁸ The computational results match the experimental measurements throughout the R_s range for $AR = 460$ and slightly overpredicts the performance of the network for $AR = 1860$ by $<4\%$ T . The discrepancy could be accounted for by adding more complexity to the MNR model, considering NW curviness and distributions of L , D , and R_{jxn} values, none of which are accounted for in the present model. A further dataset using NWs of $AR = 384$, where the model overestimates the performance of the NWN, can be found in the [supplementary material](#) (Fig. S5).

The shape of the experimentally acquired T - R_s curve is also important, as networks, which are not fully optimized through post-processing, can exhibit abnormal T - R_s profiles that deviate from the standard shape and which the MNR and MLST model can highlight.¹¹ In all cases reported here, the MNR and MLST model utilizing a $\langle R_{jxn} \rangle = 205 \Omega$ accurately predicts the performance of real world

networks. This indicates that the high-current electroforming process employed in the measurement of the single NW junctions in this work reproduces a R_{jxn} comparable to the post-processing methods employed in the fabrication of Cu NWNs.

In conclusion, we report the electrical properties of single and crossed solution-grown Cu NWs. While the material resistivity $\langle \rho \rangle$ for the Cu NWs of $20.1 \pm 1.3 \text{ n}\Omega \text{ m}$ was comparable to that of Ag NWs, the resistance of electroformed junctions $\langle R_{jxn} \rangle$ was measured to be almost $20\times$ larger at $205.7 \pm 57.7 \Omega$. Electrical characterization of individual Cu NWs enabled the electro-optical modeling of Cu NWNs, which accurately predicts the electrical and optical performance of real Cu NWNs based on physical parameters and optical constants only. These results represent a further step toward a materials-by-design approach for NWNs, investigating the fundamental material properties of individual NWs to chase the limits of performance for a collective network. We hope that this work will motivate and inform the search for processing technologies and alternate NW materials that reduce cost and environmental burden and see the full potential of NWN-based technologies realized.

See the [supplementary material](#) for SEM and TEM images of the Cu NWs used in this study including L and D distributions, a graph of the native oxide thickness with respect to NW D , threshold and LRS SET voltages vs current compliance, a plot of Q_{ext} vs NW D for Cu and Ag, and MNR and MLST data with good agreement for NWN systems with $AR = 384$.

AUTHOR'S CONTRIBUTIONS

H.G.M. wrote this paper and performed the electrical measurements and the MNR and MLST simulations. P.F.F. and M.A.C., led by B.J.W., synthesized the Cu NWs. C.G.R. and C. O'C., led by M.S.F., developed the MNR computational model. J.J.B. led overall effort. All the authors discussed and commented on this manuscript and on the results.

The authors wish to acknowledge funding from the European Research Council (ERC) under Advanced Grant No. 321160. This publication has emanated from the research supported by grants from the Science Foundation Ireland (SFI) under P.I Grant Nos. 16/IA/4462 and 18/IF/6324 and the SFI Research Centre, AMBER under Grant No. 12/RC/2278. The facilities and staff at the Advanced Microscopy Laboratory at Trinity College Dublin are greatly acknowledged for their support. The authors also acknowledge the Research IT Unit (formerly TCHPC) at Trinity College Dublin and the WestGrid (www.westgrid.ca) and Compute Canada Calcul Canada (www.computecanada.ca) for computational resources.

The authors declare no competing financial interest.

DATA AVAILABILITY

The data that support the findings of this study are available from the corresponding author upon reasonable request.

REFERENCES

- D. Bellet, M. Lagrange, T. Sannicolo, S. Aghazadehchors, V. H. Nguyen, D. P. Langley, D. Munoz-Rojas, C. Jimenez, Y. Brechet, and N. D. Nguyen, *Materials* **10**(6), 570 (2017).
- S. Ye, A. R. Rathmell, Z. Chen, I. E. Stewart, and B. J. Wiley, *Adv. Mater.* **26**(39), 6670 (2014).

- ³C. G. Rocha, H. G. Manning, C. O'Callaghan, C. Ritter, A. T. Bellew, J. J. Boland, and M. S. Ferreira, *Nanoscale* **7**(30), 13011 (2015).
- ⁴I. E. Stewart, A. R. Rathmell, L. Yan, S. Ye, P. F. Flowers, W. You, and B. J. Wiley, *Nanoscale* **6**(11), 5980 (2014).
- ⁵U. S. Geological Survey, *Mineral Commodity Summaries* (U.S. Geological Survey, 2020).
- ⁶Y. Wang and Z. Yin, *Appl. Sci. Convergence Technol.* **28**(6), 186 (2019).
- ⁷W.-H. Xu, L. Wang, Z. Guo, X. Chen, J. Liu, and X.-J. Huang, *ACS Nano* **9**(1), 241 (2015).
- ⁸S. Ye, A. R. Rathmell, I. E. Stewart, Y. C. Ha, A. R. Wilson, Z. Chen, and B. J. Wiley, *Chem. Commun.* **50**(20), 2562 (2014).
- ⁹A. T. Bellew, H. G. Manning, C. G. Rocha, M. S. Ferreira, and J. J. Boland, *ACS Nano* **9**(11), 11422 (2015).
- ¹⁰F. Selzer, C. Floresca, D. Knepe, L. Bormann, C. Sachse, N. Weiß, A. Eychmüller, A. Amassian, L. Müller-Meskamp, and K. Leo, *Appl. Phys. Lett.* **108**(16), 163302 (2016).
- ¹¹H. G. Manning, C. G. Rocha, C. O. Callaghan, M. S. Ferreira, and J. J. Boland, *Sci. Rep.* **9**(1), 11550 (2019).
- ¹²C. O'Callaghan, C. G. Rocha, H. G. Manning, J. J. Boland, and M. S. Ferreira, *Phys. Chem. Chem. Phys.* **18**(39), 27564 (2016).
- ¹³J. W. Borchert, I. E. Stewart, S. Ye, A. R. Rathmell, B. J. Wiley, and K. I. Winey, *Nanoscale* **7**(34), 14496 (2015).
- ¹⁴K. Mallikarjuna, H.-J. Hwang, W.-H. Chung, and H.-S. Kim, *RSC Adv.* **6**(6), 4770 (2016).
- ¹⁵A. R. Rathmell and B. J. Wiley, *Adv. Mater.* **23**(41), 4798 (2011).
- ¹⁶J. Schäfer, S. C. Lee, and A. Kienle, *J. Quant. Spectrosc. Radiat. Transfer* **113**(16), 2113 (2012).
- ¹⁷P. B. Johnson and R. W. Christy, *Phys. Rev. B* **6**(12), 4370 (1972).
- ¹⁸I. Valov and M. N. Kozicki, *J. Phys. D* **46**(7), 074005 (2013).
- ¹⁹H. G. Manning, S. Biswas, J. D. Holmes, and J. J. Boland, *ACS Appl. Mater. Interfaces* **9**(44), 38959 (2017).
- ²⁰R. Waser and M. Aono, *Nat. Mater.* **6**(11), 833 (2007).
- ²¹H. G. Manning, F. Niosi, C. G. Rocha, A. T. Bellew, C. O'Callaghan, S. Biswas, P. F. Flowers, B. J. Wiley, J. D. Holmes, M. S. Ferreira, and J. J. Boland, *Nat. Commun.* **9**(1), 3219 (2018).
- ²²K. D. Liang, C. H. Huang, C. C. Lai, J. S. Huang, H. W. Tsai, Y. C. Wang, Y. C. Shih, M. T. Chang, S. C. Lo, and Y. L. Chueh, *ACS Appl. Mater. Interfaces* **6**(19), 16537 (2014).
- ²³R. Waser, R. Dittmann, G. Staikov, and K. Szot, *Adv. Mater.* **21**(25-26), 2632 (2009).
- ²⁴M. M. Kolesnik, S. Hansel, T. Lutz, N. Kinahan, M. Boese, and V. Krstić, *Small* **7**(20), 2873 (2011).
- ²⁵S. Zhong, T. Koch, M. Wang, T. Scherer, S. Walheim, H. Hahn, and T. Schimmel, *Small* **5**(20), 2265 (2009).